J. Biochem. **143,** 747–758 (2008)
doi:10.1093/jb/mvn033

Structural bases for the specific interactions between the E2 and E3 components of the *Thermus thermophilus* 2-oxo acid dehydrogenase complexes

Tadashi Nakai[1,*], Seiki Kuramitsu[1,2] and Nobuo Kamiya[1,3]

[1]RIKEN SPring-8 Center, Harima Institute, Sayo, Hyogo 679-5148, Japan; [2]Department of Biology, Graduate School of Science, Osaka University, Toyonaka, Osaka 560-0043, Japan; and [3]Department of Chemistry, Graduate School of Science, Osaka City University, Sumiyoshi, Osaka 558-8585, Japan

Received January 7, 2008; accepted February 13, 2008; published online March 3, 2008

Pyruvate dehydrogenase (PDH), branched-chain 2-oxo acid dehydrogenase (BCDH) and 2-oxoglutarate dehydrogenase (OGDH) are multienzyme complexes that play crucial roles in several common metabolic pathways. These enzymes belong to a family of 2-oxo acid dehydrogenase complexes that contain multiple copies of three different components (E1, E2 and E3). For the *Thermus thermophilus* enzymes, depending on its substrate specificity (pyruvate, branched-chain 2-oxo acid or 2-oxoglutarate), each complex has distinctive E1 (E1p, E1b or E1o) and E2 (E2p, E2b or E2o) components and one of the two possible E3 components (E3b and E3o). (The suffixes, p, b and o identify their respective enzymes, PDH, BCDH and OGDH.) Our biochemical characterization demonstrates that only three specific E3•E2 complexes can form (E3b•E2p, E3b•E2b and E3o•E2o). X-ray analyses of complexes formed between the E3 components and the peripheral subunit-binding domains (PSBDs), derived from the corresponding E2-binding partners, reveal that E3b interacts with E2p and E2b in essentially the same manner as observed for *Geobacillus stearothermophilus* E3•E2p, whereas E3o interacts with E2o in a novel fashion. The buried intermolecular surfaces of the E3b•PSBDp/b and E3o•PSBDo complexes differ in size, shape and charge distribution and thus, these differences presumably confer the binding specificities for the complexes.

Key words: α-ketoacid dehydrogenase, glycine cleavage system, 2-oxo acid dehydrogenase, protein-protein interaction complex, *Thermus thermophilus*.

Abbreviations: ASA, accessible surface area; BCDH, branched-chain 2-oxo acid dehydrogenase; E3BD, E3-binding domain; GCS, glycine cleavage system; *Gst*, *Geobacillus stearothermophilus*; OGDH, 2-oxoglutarate dehydrogenase; PDH, Pyruvate dehydrogenase; PSBD, peripheral subunit binding domain; *Tth*, *Thermus thermophilus*; rms, root-mean-square.

INTRODUCTION

Pyruvate dehydrogenase (PDH), branched-chain 2-oxo acid dehydrogenase (BCDH), 2-oxoglutarate dehydrogenase (OGDH) and the glycine cleavage system (GCS) are multienzyme complexes that play crucial roles in several common metabolic pathways (e.g. glycolysis, TCA cycle and degradation of amino acids). The first three enzymes listed belong to a family of 2-oxo acid dehydrogenase complexes that contain multiple copies of three different components: 2-oxo acid decarboxylase (E1), lipoamide-containing dihydrolipoamide transacylase (E2) and lipoamide dehydrogenase (E3) (*1*); whereas GCS consists of four components: a glycine decarboxylase (P-protein), the lipoamide-containing H-protein, an aminomethyltransferase (T-protein) and a lipoamide dehydrogenase (L-protein) (*2*; Fig. 1a). The 2-oxo acid dehydrogenases and GCS catalyse oxidative decarboxylation of 2-oxo acids and glycine, respectively, in similar multistep reactions. The 2-oxo acid dehydrogenases have unique E1 (E1p, E1b or E1o) and E2 (E2p, E2b or E2o) components. (The suffixes, p, b and o identify their respective enzymes, PDH, BCDH and OGDH.) Conversely, all 2-oxo acid dehydrogenases of a given organism usually contain the same E3 component. Moreover, it is often the case that the same enzyme acts as both the E3 component of the dehydrogenases and the GCS L-protein (*3*). However, several organisms possess more than one E3 and when this occurs, each is the exclusive component of a dehydrogenase or GCS (*1*). In the genome of *Thermus thermophilus* (*Tth*) HB8, whose dehydrogenase E2 and E3 components are the focus of this study, we found two open reading frames with sequences that are homologous to those of known E3 component genes. The biochemical properties of these E3 isozymes have not yet been characterized.

In all 2-oxo acid dehydrogenase complexes, the E2 components (E2s) are assembled into either a cubic (24-mer) or a dodecahedral (60-mer) inner core, around which E1 and E3 components (E1s and E3s, respectively) bind. Each E2 is a highly segmented structure composed of three independently folded domains: one or more N-terminal lipoyl domains (~80 residues); a peripheral

*To whom correspondence should be addressed. Tel: +1-206-616-4510, Fax: +1-206-685-7002, E-mail: nakaix@u.washington.edu

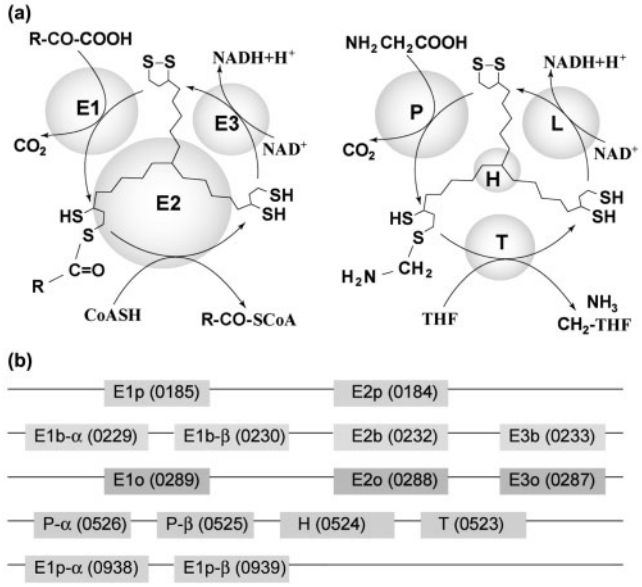

Fig. 1. **Reaction mechanisms for and gene clusters of the 2-oxo acid dehydrogenase complexes and the glycine cleavage system.** (a) Reaction mechanisms for the 2-oxo acid dehydrogenases (left) and the glycine cleavage system (right). (b) Gene clusters of the 2-oxo acid dehydrogenases and the glycine cleavage system in the *Tth* genome. Values in parentheses are the gene numbers. Addition of the prefix TTHA to each gene number produces the corresponding KEGG accession ID (e.g. TTHA0233 for E3b). Assignment of the genes is based on the KEGG annotation database except for TTHA0232 and TTHA0233, which were initially annotated as E2p and E3p, respectively. The reaction mechanism diagrams are adapted from Cohen-Addad *et al*. (*34*).

subunit binding domain (PSBD, ~35 residues); and a C-terminal catalytic domain (~250 residues). The domains are connected by highly flexible linker regions of ~25–40 residues. Each PSBD binds tightly to E1 *or* E3, thereby studding the surface of the inner core with E1s and E3s. On the other hand, in eukaryotic PDH complexes, a separate protein (the E3-binding protein) that is bound non-covalently to the inner core and contains a PSBD-like domain, binds E3 exclusively. Crystal and/or solution structures have been determined for E1bs (*4–6*); E1ps (*7*, *8*); E1o (*9*); and E3s (*10–17*); for the lipoyl domains of E2p (*18–21*) and of E2o (*22*); for PSBD of E2o (*23*) (PSBDo) and PSBDp (*24*); and for the cubic (*25*, *26*) and the dodecahedral (*27*) inner cores of E2p. Furthermore, crystal structures exist for the complexes, E3•PSBDp (*28*); E1p•PSBDp (*29*); and E3 with the E3-binding domain (E3BD) of the eukaryotic E3-binding protein (*30*, *31*).

In comparison with the 2-oxo acid dehydrogenases, the interactions among the components of GCS are rather weak. *In vivo*, GCS is a stable complex with its components in an approximate ratio of 2P:27H:9T:1L (*32*); whereas, *in vitro*, it easily dissociates into its component proteins and the H-protein then acts as a mobile cosubstrate that commutes among the other three enzymes (*32*). Crystal structures of the P-protein (*33*), the H-protein (*34*, *35*), the T-protein (*36–38*) and the L-protein (*10–17*) have been reported, but there are, as yet, no three-dimensional

```
          130       140       150       160
            L0 <--H1---> L1 <#>     L2    <--H2-->
PSBDp .PAAPSIRRLARELGVDLTRLRGTGLAGRITEEDVRRAAGL
PSBDb MLAVPAARKLARELGIPIEEVPGSGPLGRVRVEDVRAYAER
PSBDo .LAMPAAERLMQEKGVSPAEVQGTGLGGRILKEDVMRHLEE
          * *: .:* :* *:    .: *:*  **:  ***
E3b·PSBDp ^^^^^ ^^  ^^                 ^  ^
E3b·PSBDb ^^^^^ ^^  ^^                 ^ ^^^
E3o·PSBDo ^^^^^ ^^  ^^           ^^^   ^ ^^^  ^
```

Fig. 2. **Amino-acid sequence alignments of the three Tth E2 PSBDs.** Above the alignments are secondary-structure assignments for PSBDp, with its short 3_{10}-helix indicated by '#'. Identical residues are marked with asterisks. Colons and periods indicate conserved and semi-conserved substitutions, respectively. PSBD residues that interact with E3 are indicated by '^'. The PSBD residue numbers mimic the *Gst* E2p sequence numbers in order to facilitate comparisons.

structures for any of the possible complexes that could be formed by these components.

E3 (NADH:lipoamide oxidoreductase, EC 1.8.1.4) is a homodimeric (~100 kDa) FAD-dependent disulfide reductase. This enzyme catalyses the NAD^+-dependent oxidation of the dihydrolipoyl that is covalently linked to E2 or, when acting as the L-protein, catalyses the same reaction using the dihydrolipoyl of the H-protein. As implied previously, in most organisms, E3 is encoded by a single gene and is shared among the various 2-oxo acid dehydrogenases and GCS. However, the *Tth* genome encodes two homologous E3 genes. One gene is located in the gene cluster encoding the BCDH components. The other is located in the operon encoding the OGDH components (Fig. 1b). On the basis of this information and their biochemical properties described below, we refer to the gene products as E3b and E3o, respectively. E3b and E3o have 464 and 455 residues, respectively, and exhibit 49% sequence identity. They also have 48% and 43% sequence identities, respectively, with E3 from *Geobacillus stearothermophilus* (*Gst*), a close homologue with a known three-dimensional structure. The PSBDs of the three *Tth* E2s contain 40 or 41 amino-acid residues and exhibit the same amount of sequence identity (45%) between any pair of them (Fig. 2).

Herein we report the biochemical characterization of E3b, E3o, PSBDp, PSBDb and PSBDo from *Tth*, and the crystal structures of three E3•PSBD complexes. Our biochemical analyses of the interactions between the various E3s and the PSBDs reveal that each PSBD parent E2 targets only one of the two E3s, so that only three different complexes (E3b•E2p, E3b•E2b and E3o•E2o) can exist. The complexes (E3b•PSBDp, E3b•PSBDb and E3o•PSBDo) were crystallized and their structures solved using X-ray crystallography. Examination of their structures reveals that E3b interacts with PSBDp and PSBDb in essentially the same manner as observed for *Gst* E3•PSBDp (*28*); whereas E3o interacts with PSBDo in a novel fashion. Our data provide structural bases for the species-specific binding of the *Tth* E2•E3 complexes.

EXPERIMENTAL PROCEDURES

Protein Expression—Construction of the plasmids was carried out in the *E. coli* strain, DH5α. Based on the

amino-acid sequence of PSBDb, two oligonucleotides (5′-G GAA TTC CAT ATG TTG GCT GTT CCG GCT GCT CGT AAA CTG GCT CGT GAA CTG GGT ATC CCG ATC GAA GAA GTT CCC GGG TCT GGT CCG CTG GGT CGT GTT CGT GTT GAA GAC GTT CGT GCT TAC GCT GAA CGT TAA TAA GGA TCC CG-3′ and its complement) were synthesized by Greiner Bio-One. The oligonucleotides were annealed and digested at the *Nde*I and *Bam*HI sites (underlined), and the resulting DNA fragment containing the gene encoding PSBDb was inserted between the same two sites in pET-11a (Novagen). The resulting plasmid was transformed into the expression host *E. coli* BLR(DE3). Cultivation and target gene expression were performed according to the pET system manual (Novagen). Cells were grown at 37°C in Luria–Bertani medium containing 50 μg/ml ampicillin. These cultures were induced with 1.0 mM isopropyl-β-D-thiogalactopyranoside when their optical densities (at 600 nm) reached 0.5–0.8 and then were incubated for an additional hour, after which the cells were harvested.

The expression plasmids pET11a-TTHA0233 and pET11a-TTHA0287, containing the genes for E3b and E3o, respectively, were supplied by the RIKEN Structural Genomics Initiative (*39*). Cultivation and expression were performed as for PSBDb except that cells were harvested 3 h after induction.

Protein Purification—All purification steps were performed on ice or at 4°C and all chromatography resins were purchased from GE Healthcare Bio-Sciences, unless otherwise noted. The purification procedures for the two E3s were essentially identical. A cell pellet containing expressed E3b or E3o was suspended in 10 mM sodium phosphate (pH 7.0), 5 mM 2-mercaptoethanol, 50 mM NaCl, and then disrupted by sonication. The cell lysate was incubated at 70°C for 10 min, kept on ice for 12 min, and then centrifuged (9,400*g*) for 60 min. Ammonium sulfate was added to the resulting supernatant to a final concentration of 1.2 M, after which the solution was applied to a Resource PHE column (6 ml) equilibrated with 50 mM sodium phosphate (pH 7.0), 1.2 M ammonium sulfate. Protein was eluted with a linear gradient of 1.2–0 M ammonium sulfate in 50 mM sodium phosphate (pH 7.0). Fractions containing the target protein were collected and desalted over a HiPrep 26/10 desalting column equilibrated with 10 mM sodium phosphate (pH 7.0). The sample was next applied to a Resource Q column (6 ml) equilibrated with the same buffer and protein was then eluted with a linear gradient of 0–500 mM NaCl. Fractions containing the target protein were desalted and applied to a hydroxyapatite column CHT5-I (5 ml; Bio-Rad) that was equilibrated with 10 mM sodium phosphate (pH 7.0). Protein was eluted with a linear gradient of 10–500 mM sodium phosphate (pH 7.0). Fractions containing the target protein were then loaded onto a HiLoad 16/60 Superdex 200 prep grade column equilibrated with 10 mM sodium phosphate (pH 7.0), 150 mM NaCl and eluted with the same buffer. The peak fractions were pooled and concentrated to 10 mg/ml in 20 mM HEPES-NaCl buffer (pH 7.5) using a Vivaspin concentrator (30 kDa cut-off; Sartorius).

For purification of PSBDb, a cell pellet was suspended, disrupted and heat-treated as were the E3 cell pellets. The resulting supernatant was applied to a HiTrap SP column (5 ml) equilibrated with 10 mM sodium phosphate (pH 7.0). Protein was then eluted with a linear gradient of 0–500 mM NaCl. Fractions containing the target protein were desalted and applied to a Resource S column (6 ml) equilibrated with 10 mM sodium phosphate (pH 7.0). Protein was eluted with a 0–500 mM NaCl gradient. Fractions containing the target protein were then loaded onto a HiLoad 16/60 Superdex 75 prep grade column equilibrated with 10 mM sodium phosphate (pH 7.0), 150 mM NaCl and eluted with the same buffer. The peak fractions were pooled and concentrated to 2 mg/ml with a Vivaspin concentrator (3 kDa cut-off).

Two 40-residue peptides corresponding to PSBDp and PSBDo were synthesized by Greiner. The composition and purity (>95%) of each were verified by HPLC and mass spectrometry. The peptides, received as lyophilized materials, were dissolved in 100 mM Tris–HCl (pH 8.5) at concentrations of 2 mg/ml.

H-protein was expressed and purified as described by Nakai *et al*. (*35*). The purification involved a heat treatment and three column chromatographies. Since the resulting H-protein preparation was a mixture of apo and holo (lipoyl) forms (*35*), each form was isolated by an additional chromatography step. The mixture was applied to a Mono Q column (1 ml) equilibrated with 10 mM sodium phosphate (pH 7.0) and the proteins were eluted with a linear gradient of 250–500 mM NaCl. The identity of each form was confirmed by mass spectrometry.

The E3•PSBD complexes were obtained by ultrafiltration. An E3 was mixed with a 2-fold molar excess of a PSBD and incubated at 25°C for 30 min. Excess PSBD was removed by three subsequent exchanges with 20 mM HEPES–NaOH (pH 7.5) using a Vivaspin concentrator equipped with a membrane with a 30 kDa cut-off.

Assay of Enzymatic Activity—The activities of E3s were measured at 20°C as described by Neuburger *et al*. (*40*) with minor modifications. The assay mixture contained 50 mM Tris–HCl (pH 7.7), 8 mM TCEP (a reducing agent, whose inclusion insures the full reduction of substrate), known amounts of substrate (lipoamide or H-protein) and 3 mM NAD^+ in a final volume of 100 μl. Reactions were initiated by adding 10 nM E3b or E3o. The progress of the reaction was monitored by measuring the increase in absorbance at 340 nm that occurs upon reduction of NAD^+. Kinetic parameters, k_{cat}, K_m and k_{cat}/K_m, were determined from Hanes–Woolf plots. Substrate concentrations were varied so that K_m values were flanked by six data points.

Crystallization and Data Collection—All crystallization experiments, unless otherwise noted, were performed at 18°C using the hanging drop vapour diffusion method, for which 2 μl of a 10 mg/ml protein solution was mixed with an equal volume of the reservoir solution and equilibrated against 500 μl of the reservoir solution. Crystals of E3b•PSBDb were grown with a reservoir solution consisting 30% (w/v) PEG MME 5000, 200 mM ammonium sulfate, 100 mM MES–NaOH (pH 6.5). Crystals of E3b•PSBDp were grown with a reservoir solution consisting of 14% (w/v) PEG 3350, 100 mM HEPES (pH 7.5). Crystals of E3o•PSBDo were grown with a reservoir solution

Table 1. **Data collection, refinement and model statistics.**

	E3b•PSBDp	E3b•PSBDb	E3o•PSBDo
Data collection			
Beamline	BL45XU, SPring-8	BL45XU, SPring-8	BL44B2, SPring-8
Wavelength (Å)	1.00	1.00	1.00
Space group	$P2_1$	$P1$	$P2_12_12_1$
Unit-cell parameters			
a/*b*/*c* (Å)	85.8/104.1/112.9	88.8/88.9/144.1	85.0/107.1/131.7
$\alpha/\beta/\gamma$ (°)	90.0/107.3 /90.0	89.3/87.0/70.8	90.0/90.0/90.0
Resolution range[a] (Å)	50.0–1.94 (2.01–1.94)	50.0–2.09 (2.16–2.09)	50.0–1.80 (1.86–1.80)
No. of measured reflections	523,077	468,118	796,589
No. of unique reflections	139,010 (13,440)	238,181 (21,564)	111,571 (10,985)
Redundancy[a]	3.8 (3.7)	2.0 (1.8)	7.1 (6.6)
Completeness[a] (%)	99.1 (96.3)	96.8 (87.4)	99.8 (99.6)
R_{merge}[a,b] (%)	4.7 (15.7)	3.8 (25.6)	7.5 (41.3)
Average I/σ[a] (I)	39.1 (10.2)	18.3 (1.7)	25.6 (3.6)
Refinement			
Resolution range[a] (Å)	50.0–1.94 (2.06–1.94)	50.0–2.09 (2.16–2.09)	39.1–1.80 (1.91–1.80)
R_{work}[a]	0.207 (0.240)	0.217 (0.281)	0.207 (0.247)
R_{free}[a]	0.244 (0.286)	0.257 (0.316)	0.238 (0.273)
Model			
Deviations			
Bond lengths (Å)	0.005	0.006	0.005
Bond angles (°)	1.2	1.3	1.2
Mean B factors			
Main-chain atoms for E3[c] (Å^2)	24.40 (1,840)	40.28 (3,680)	16.46 (904)
Side-chain atoms for E3 (Å^2)	27.42	43.14	21.15
Main-chain atoms for PSBD[c] (Å^2)	28.35 (78)	69.18 (160)	62.05 (37)
Side-chain atoms for PSBD (Å^2)	32.57	68.96	63.79
FAD atoms[c] (Å^2)	21.90 (4)	36.40 (8)	11.31 (2)
NAD^+ atoms[c] (Å^2)	—	—	29.92 (2)
Water atoms[c] (Å^2)	39.15 (1,889)	41.13 (1,007)	40.94 (1,159)
Ramachandran plot			
Favored	1,431	2,837	730
Additional allowed	131	282	61
Generously allowed	1	1	1
Disallowed	1	0	0

[a]Numbers in parentheses correspond to those found for the highest resolution shell. [b]$R_{merge} = \Sigma_{hkl}\ \Sigma_i\ |\ I_{hkl,i} - \langle I_{hkl}\rangle\ |\ /\ \Sigma_{hkl}\ \Sigma_i\ I_{hkl,i}$, where I is the observed intensity and $\langle I\rangle$ is the averaged intensity for multiple measurements. [c]Numbers in parentheses correspond to the number of residues or molecules. Owing to poor electron density, the following N- or C-terminal residues were not included in the final models: Met4–Pro6 and Arg470 for all E3b models; E3o Ile453–Leu455 for E3o•PSBDo; and PSBDp Gly169, PSBDb Glu169, and PSBDo Leu167–Glu169 for models containing those molecules.

consisting 45% (v/v) MPD, 200 mM NaCl and the addition of 1 µl of 20 mM NAD^+ to the initial drop.

Prior to data collection, each crystal was soaked for a few seconds in a cryoprotectant solution, then transferred to a nylon loop, and flash-cooled in a nitrogen gas stream at 90 K. The cryoprotectants were the reservoir solution plus PEG 400 (for E3b•PSBDb) or PEG 3350 (for E3b•PSBDp). For E3o•PSBDo, the mother liquor was an adequate cryoprotectant. X-ray diffraction data were collected at 90 K using synchrotron radiation from BL45XU (*41*) or BL44B2 (*42*) at SPring-8 (Table 1). Data processing was completed using the program HKL2000 (*43*; Table 1).

Structure Determination and Refinement—The structures of E3b•PSBDp and E3b•PSBDb were solved by the molecular-replacement method with the program AMoRe (*44*), using *Tth* E3b (PDB entry 2EQ6; Kondo, H. *et al.*, unpublished data) as the search model. The model was constructed from the dimeric molecule, with all water molecules removed. Structure factors in the 15–4 Å resolution range were used for the searches. The structure of E3o•PSBDo was solved using the same protocol, except that *Tth* E3o (PDB entry 2YQU; Kondo, H. *et al.*, unpublished data) was used as a search model.

All structures were refined using the program CNS (*45*). For the initial model of each E3•PSBD complex, all E3 side chains and FAD molecules were included. Rigid-body refinement was carried out with the dimer as a rigid body and then, each subunit was allowed to move independently. Each electron density map produced at this stage of refinement was of good quality and the models of the PSBD molecules were gradually built into the electron density maps through several cycles of model building using the program, XtalView (*46*). Subsequent structure refinements were carried out by simulated annealing and energy minimization. After several rounds of refinement and manual rebuilding,

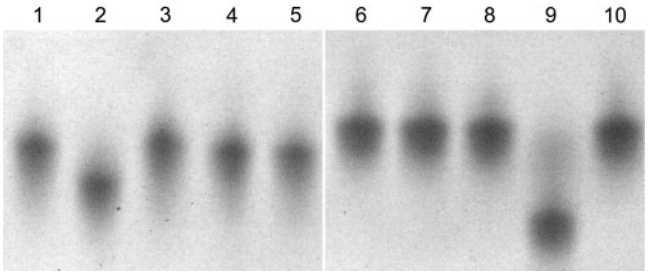

Fig. 3. **Non-denatured gel mobility shift assays of E3•PSBD complexes.** Ten micrograms of E3b (lanes 1–5) or E3o (lanes 6–10) were loaded alone (lanes 1, 5, 6 and 10) or with 1 μg of PSBDb (lanes 2 and 7), PSBDp (lanes 3 and 8) or PSBDo (lanes 4 and 9) onto a 10% polyacrylamide gel in 5 mM Tris–Tricine gel buffer (pH 8.6). Samples were incubated for 30 min before loading them onto the gel and then were electrophoresed at 150 V for 120 min.

water molecules were identified in the difference maps based on peak heights and distance criteria. Further model building and refinement cycles produced the final models.

Analyses of the stereochemistries showed that all of the models were of good quality, with virtually all of the residues' ϕ-φ values found within allowed regions of Ramachandran plots (Table 1). The peptide bonds of the E3b proline residues, 319, 356 and 447, and the E3o proline residues, 356 and 447, have *cis* conformations. Refinement statistics are summarized in Table 1 and the final electron density maps are shown in Fig. S1.

Graphical representations of the protein structures were generated using MOLSCRIPT (*47*; Figs 4–8 and S1), Xfit (*46*; Figs 5 and S1) and GRASP (*48*; Fig. 6), and rendered using Raster3d (*49*). Coordinates and structure factors have been deposited in the Protein Data Bank with the accession codes 2EQ8, 2EQ9 and 2EQ7 for E3b•PSBDp, E3b•PSBDb and E3o•PSBDo, respectively.

RESULTS AND DISCUSSION

Binding of the PSBDs to the E3s—To determine the binding affinities of the three PSBDs to E3b and E3o, gel mobility shift assays were performed (Fig. 3). Obviously, since the respective binding partner was present, the gel positions of E3b and E3o in the presence of PSBDb and PSBDo, respectively, shifted. The migration rates are faster than those of the isolated E3s; whereas E3b with PSBDp present migrated slightly more slowly than it did in the absence of PSBDp. The calculated isoelectric point of PSBDp (pI = 11.52) is higher than those of PSBDb (8.34) and PSBDo (5.23), and the pH of the electrophoretic buffer (8.6). These values are consistent with a slower migration for an E3b•PSBDp complex and faster migrations for E3b•PSBDb and E3o•PSBDo complexes as found experimentally. The formation of specific E3•PSBD complexes was also confirmed by the results of ultrafiltration experiments. We expected and found that the PSBDs (~4.3 kDa) would pass through membranes of 30 kDa cut-off unless bound to an E3. For all possible E3•PSBD arrangements, only E3b•PSBDp, E3b•PSBDb and E3o•PSBDo were isolated from the ultrafiltration retentates. Crystals of these complexes, which were isolated from the retentates, were used to determine their structures (see below).

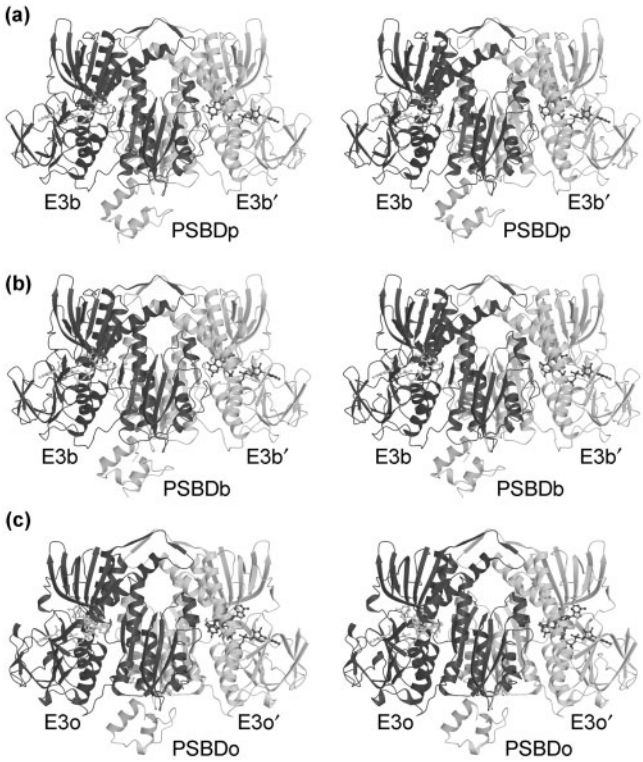

Fig. 4. **Stereoviews of the overall structures of E3•PSBDs.** (a) E3b•PSBDp; (b) E3b•PSBDb; (c) E3o•PSBDo. FAD and NAD^+ molecules are shown as ball-and-stick models.

Enzymatic Activities of E3b and E3o and Their Binding Affinities to H-protein—The enzymatic activities of E3b and E3o were measured using lipoamide and H-protein as substrates (Table 2). The kinetic constants of E3b and E3o are similar no matter which substrate was used. Thus, given their enzymatic activities, both E3b and E3o seem to function equally well as L-proteins. This finding contrasts with what is found for the *Pseudomonas putida* isozymes, for which one E3 is specific for GCS and is five times more active than the other E3 when the H-protein is the substrate (*50*). However, the large difference in the activities of the *P. putida* E3s might be exceptional and caused by specific structural interactions. For the pea L- and H-proteins specific structural interactions do not seem to be required for activity (*40*). Likewise, the *Tth* GCS may not require structure-specific interactions between E3 and the H-protein.

For the 2-oxo acid dehydrogenases, the E2 lipoyl domain corresponds to the GCS H-protein. The 130-residue H-protein is essentially an 80-residue lipoyl domain with 20-residue extensions at both ends. Recently, Fries *et al*. (*51*) have shown, by NMR spectroscopy, that there are no specific interactions between E3 and the E2 lipoyl domain of the *Gst* PDH complex. Their data support the ideas that PSBD, and not the lipoyl domain, is crucial for the formation of a stable complex between E2 and E3 and that the GCS H-protein,

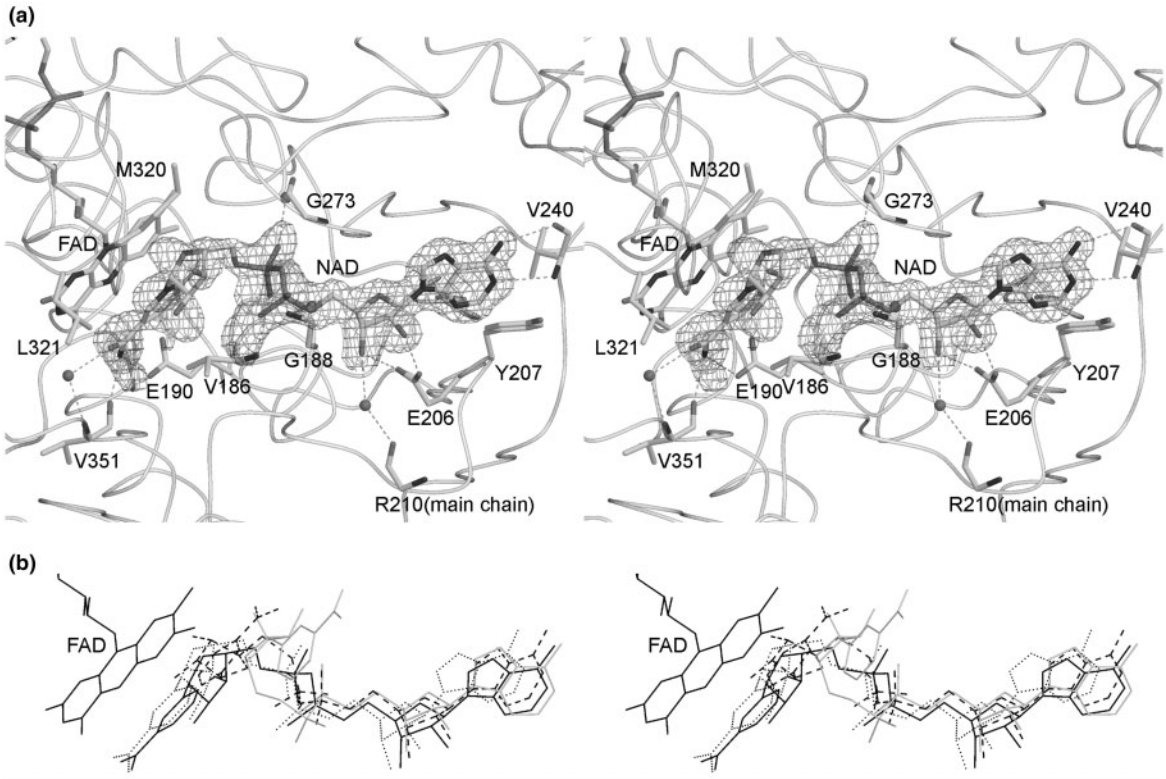

Fig. 5. **Stereoviews of NAD$^+$ and NADH when bound to E3s.** (a) The NAD$^+$ electron density map for *Tth* Eo•NAD$^+$. The simulated-annealing omit map was calculated starting at 1000 K, without the NAD$^+$ molecule, and contoured at the 3.0σ level. (b) The conformations of NAD$^+$ and NADH when bound to E3s. The structures of *Tth* E3o•NAD$^+$ (solid), human E3•NAD$^+$ (gray), human E3•NADH (dotted) and *P. putida* E3•NAD$^+$ (broken) are superimposed using only the E3 Cα atoms. The resulting conformations of the NAD$^+$s and NADH are shown. For reference, the FAD of the E3o•NAD$^+$ structure is also shown.

as a lipoyl domain, does not have structure-specific interactions with the L-protein. Therefore, the absence of a PSBD counterpart in GCS accounts for the lack of a stable complex between the GCS H- and L-proteins.

Descriptions of the E3•PSBD structures—The crystal structures of the three complexes (E3b•PSBDp, E3b•PSBDb and E3o•PSBDo) were analyzed (Fig. 4). For each complex, the E3 molecule has an α_2 dimeric structure related by a non-crystallographic twofold axis and shares a similar three-dimensional structure with all other known E3 structures. The root-mean-square (rms) deviations calculated for the Cα positions are 1.6 Å (E3b vs. E3o), 1.7 Å (E3b vs. *Gst* E3) and 1.6 Å (E3o vs. *Gst* E3). Like all other E3s, the *Tth* E3s are composed of four structurally distinctive parts: the FAD-binding domain (residues 4–147); the NAD$^+$-binding domain (residues 148–276); the central domain (residues 277–345); and the interface domain (residues 347–470). (The numbering of the *Tth* E3b and E3o residues mimics that of *Gst* E3 so that facile comparisons can be made.) Each E3 dimer has two active-site pockets at the subunit interface. The FAD cofactor is bound by extensive non-covalent interactions with residues from both subunits. Most of the important residues involved in catalysis and near the cofactor are conserved among the *Tth* E3 isozymes as well as all other E3s with known structures.

In the three *Tth* E3•PSBD structures, each E3 dimer binds a single PSBD (Fig. 4). The overall folds and the secondary structure elements are essentially the same for the three PSBDs. The structure of each PSBD has the following elements: two short parallel α-helices (H1 and H2); a short 3_{10}-helix or (for PSBDo) β-turn that is perpendicular to the α-helices; two loops (L1 and L2) joining these structural elements, and an N-terminal loop (L0) (Figs 2 and 7). H1 and H2, pack against each other with extensive hydrophobic interactions. Along with a few hydrophobic residues from L1 and L2, the two α-helices form the core of the domain. These structural features are essentially the same as those of other PSBDs with known structures. PSBD is one of the smallest globular domains known that is not stabilized by disulfides or metal ions (*52*, *53*).

Since the asymmetric units of the E3b•PSBDp and E3b•PSBDb crystals contain two and four complexes, respectively, the structure determinations give independent results for two PSBDps and four PSBDbs. All PSBD structures are quite similar. Least-squares fits of all of the corresponding Cα atoms in the two PSBDps and four PSBDbs give average rms deviations of 0.153 and 0.282 Å, with maximum displacements of 0.357 and 0.842 Å, respectively, except for the C-terminal Gly168 of PSBDp. The average B factors for the main-chain atoms of PSBDp are 26.9 and 29.8 Å^2 for molecules

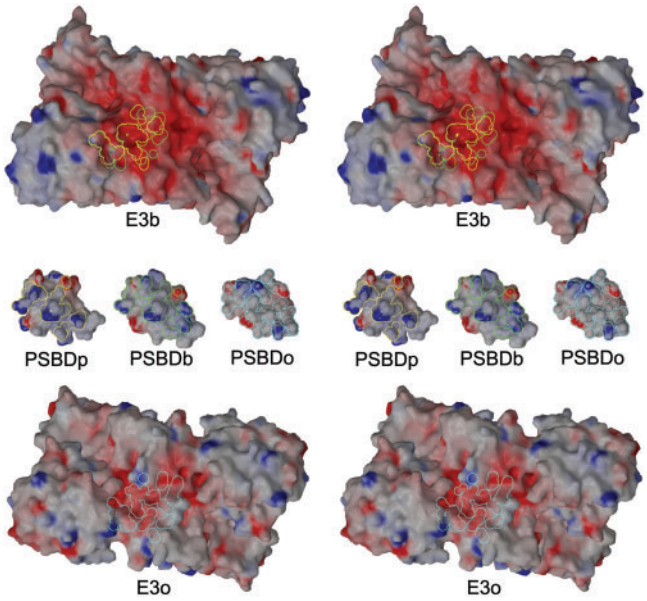

Fig. 6. **Stereoviews of the electrostatic potential surfaces of the E3s and PSBDs at the binding interfaces.** The E3s and PSBDs are rotated by 90° out of the plane of Fig. 4 such that the binding surfaces are visible. The molecular surfaces buried in E3b•PSBDp, E3b•PSBDb and E3o•PSBDo are outlined with yellow, green and cyan curves, respectively. The negative and positive charges are represented in red and blue, respectively.

C and F, respectively; while those of PSBDb are 55.7, 73.7, 72.5 and 74.8 Å^2 for molecules C, F, I and L, respectively. Since the C molecules of PSBDp and PSBDb have the lowest B values and therefore less atomic disorder, the structures of those molecules were analysed.

Binding of NAD$^+$ to E3o—The best diffracting E3o•PSBDo crystals were obtained using NAD$^+$ as a crystallization additive. Electron density for the NAD$^+$ molecule was identified in the NAD$^+$-binding pocket of E3o (Fig. 5a). The NAD$^+$ molecule interacts with the protein through hydrogen bonds and hydrophobic contacts and its conformation is stabilized by these interactions. Several crystal structures of E3s in complex with NAD$^+$ or NADH have been reported. They are E3•NAD$^+$s from *P. putida* (*11*) and *Saccharomyces cerevisiae* (PDB entry 1V59; there is no associated publication), and human E3•NAD$^+$ and E3•NADH (*16*). Superimposition of these structures, by least-squares fitting of the Cα atoms, shows that the conformation of NAD$^+$ observed for *Tth* E3o•NAD$^+$ is essentially the same as the conformation of NADH observed for human E3•NADH (Fig. 5b). Interestingly, it is different from those of the other E3•NAD$^+$s. The conformations of the nicotinamide portions of the NAD$^+$ molecules bound to *Tth*, *P. putida* and human E3s are most dissimilar. For the *S. cerevisiae* E3•NAD$^+$ complex, the nicotinamide moiety is not included in the model, apparently because its electron density map is not well defined. Similarly, for *Tth* E3o•NAD$^+$ and the other E3•NAD$^+$s, the electron densities for the nicotinamide moieties are weaker than those for the adenosine moieties. The average B factors of the atoms in the former and the latter are 41.0 Å^2 and 19.5 Å^2, respectively. In contrast, the corresponding values for the nicotinamide and adenosine moieties of human E3•NADH are 39.9 Å^2 and 38.3 Å^2, respectively (*16*). Therefore, although the conformations of the NAD$^+$ molecules differ for *Tth* E3o•NAD$^+$ and the other E3•NAD$^+$s, the nicotinamide moiety of NAD$^+$ always has a greater conformational flexibility.

Interactions of PSBDs with E3s—For all three *Tth* E3•PSBDs, one PSBD is bound to one E3 dimer (Fig. 4). Each PSBD is bound across the twofold symmetry axis of the E3 dimer. This explains why these homodimers bind only one PSBD, as do *Gst* E3 (*28*) and *Gst* E1p (*29*) to their respective PSBDs, and human E3 to E3BD (*30*, *31*). The 1:1 stoichiometry contrasts with the expectation that, in general, a homodimer would have two binding sites. The interface accessible surface areas (ASAs) for the PSBDs of E3b•PSBDb, E3b•PSBDp and E3o•PSBDo are approximately 664, 628 and 832 Å^2, respectively. About 21%, 22% and 32% of the total PSBD ASAs (3,225, 2,919 and 2,641 Å^2), respectively, are therefore buried (Fig. 6). The interface ASAs for the PSBDs and E3s are predominantly positively and negatively charged, respectively, resulting in electrostatic complementarity. For all E3•PSBDs, each PSBD interacts with both E3 monomers through salt bridges, hydrogen bonds and hydrophobic contacts (Fig. 7 and Table S1).

Comparison of the E3b•PSBDp and E3b•PSBDb structures—The PSBD-binding site of E3b consists mostly of residues from the interface domain, while the PSBD residues involved in binding to E3b are from two regions: region 1 (R1) composed of L0 and H1, and region 2 (R2) composed of L2 and H2 (Fig. 2). The contribution of R1 to binding is greater than that of R2. The interface ASAs of R1s of PSBDp and PSBDb are 579 and 487 Å^2, and those of R2s are 85 and 141 Å^2, respectively.

Both E3b complexes are stabilized mainly by electrostatic interactions. All PSBD residues that form salt bridges with E3b are situated in R1. Arg136bd (the suffix 'bd' indicates that it is a PSBD residue) contributes important stabilizing electrostatic interactions. Its guanidinium group forms salt bridges with the E3b Asp344 and Glu431 carboxylates. The guanidinium of Arg140bd forms a salt bridge with the carboxylate and a hydrogen bond with the main-chain carbonyl of Asp340. The conformations of the Asp344 and Asp340 side chains that are involved in PSBD binding differ from those of the second E3b subunit that do not participate in binding. These conformational alterations facilitate salt bridge formation with the relevant PSBD side chains. The guanidinium of Arg157bd forms a hydrogen bond with the main-chain carbonyl of Met432. The main-chain NH of Ser134bd (Ala in PSBDb) forms a hydrogen bond with the carboxylate of Asp438′. (A prime after a residue number indicates that the residue belongs to the second E3b subunit). In addition to these interactions that are common to both E3b complexes, the following interactions are specific to each complex. For E3b•PSBDp, the guanidinium of Arg137bd forms a hydrogen bond with the hydroxyl of Tyr345. For E3b•PSBDb, the guanidiniums of Arg157bd and Arg159bd form hydrogen bonds with the main-chain carbonyls of Gly433 and Met432′, respectively.

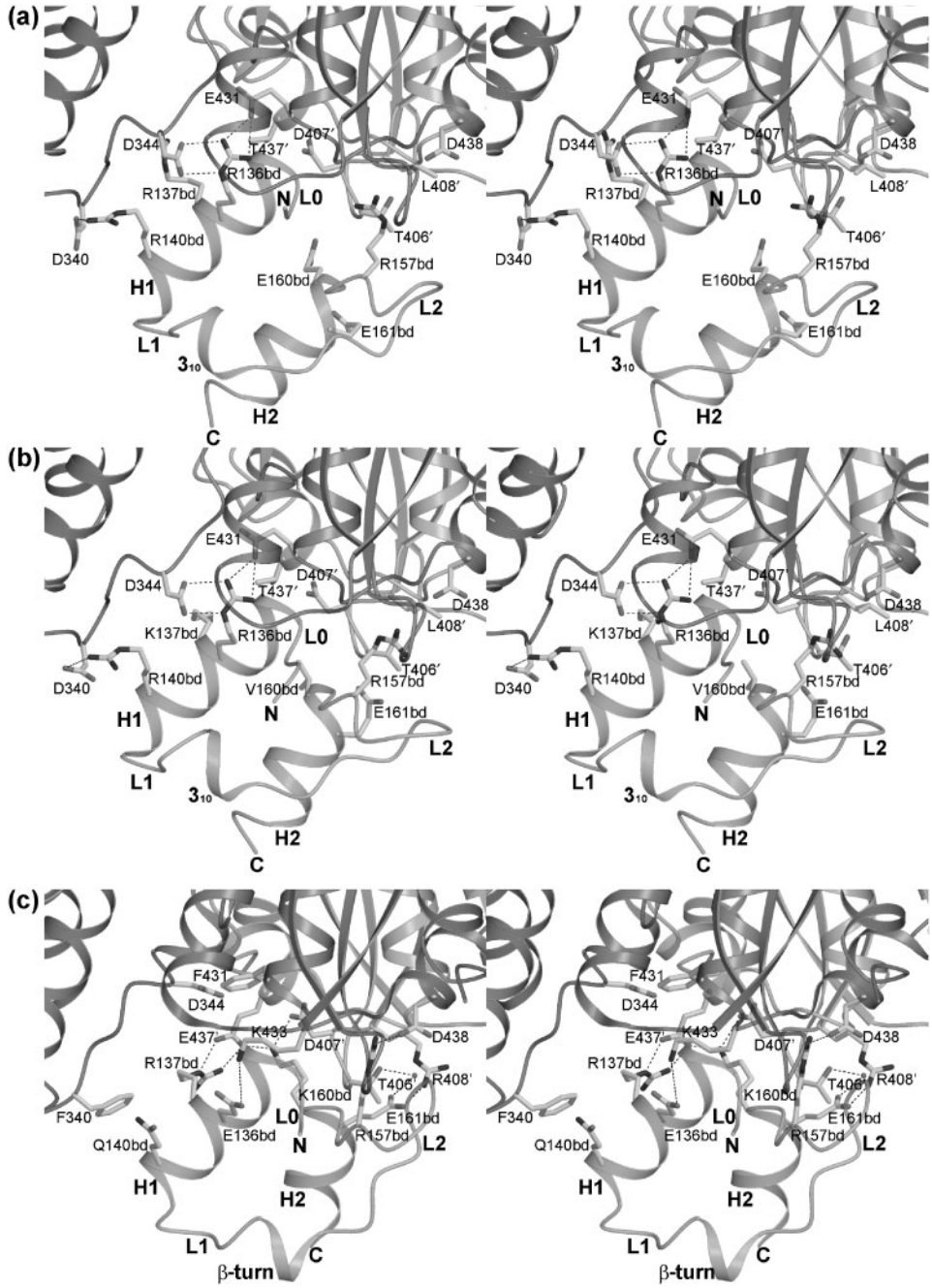

Fig. 7. **Stereoviews diagramming E3 and PSBD interactions.** (a) E3b•PSBDp; (b) E3b•PSBDb; (c) E3o•PSBDo. The orientations are the same as those of Fig. 4.

Unique structural features of E3o•PSBDo—The PSBD-binding site of E3o also consists mostly of interface domain residues, while the PSBDo residues involved in binding to E3o are from R1 and R2 as they are for the E3b•PSBDs (Fig. 2). In contrast to the other complexes, the R1's binding contribution is less than that of R2; the interface ASAs of R1 and R2 are 391 and 441 Å^2, respectively.

As is true of the E3b•PSBDs and the other complexes (*28*, *30*, *31*), the E3o•PSBDo complex is stabilized by electrostatic interactions. However, the interactions are different from those found for the other complexes. The PSBDo residues that form salt bridges with E3o are situated in H1, H2 and L2. In H1, the guanidinium of Arg137bd forms a salt bridge with the carboxylate of Glu437′. Additionally, the carboxylate of Glu136bd forms a weak electrostatic interaction with the amino of Lys433. (The distance between the carboxylate oxygens and the amino nitrogen is 5.0 Å.) The guanidinium of Arg157bd, a L2 residue, forms a salt bridge with the

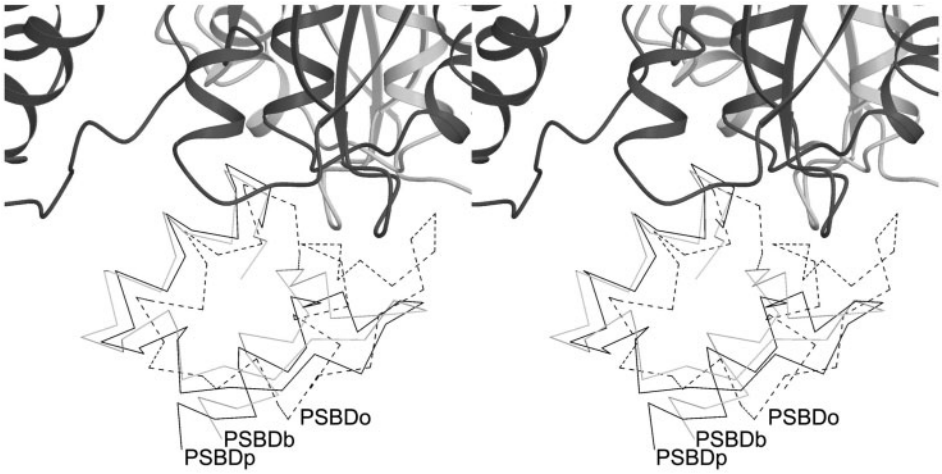

Fig. 8. **Superimposed stereoviews of the three *Tth* PSBDs.** The structures of PSBDp, PSBDb and PSBDo were superimposed using only the Cα atoms of E3b and E3o. For reference, E3b of the E3b•PSBDp complex is shown. The orientation is the same as that in Fig. 4.

Table 2. **Kinetic parameters for E3b and E3o.**

Substrate	Enzyme	K_m (μM)	k_{cat} (s^{-1})	k_{cat}/K_m ($M^{-1}s^{-1}$)
H-protein	*Tth* E3b	5.1 ± 0.2	38 ± 1	$75 \pm 4 \times 10^5$
	Tth E3o	5.9 ± 0.2	63 ± 2	$106 \pm 5 \times 10^5$
	pea E3[a]	27 ± 3	345 ± 10	$130 \pm 20 \times 10^5$
Lipoamide	*Tth* E3b	45 ± 1	37 ± 1	$8.1 \pm 0.3 \times 10^5$
	Tth E3o	53 ± 2	33 ± 2	$6.2 \pm 0.4 \times 10^5$
	pea E3[a]	500 ± 50	190 ± 20	$7.6 \pm 0.2 \times 10^5$

[a]Values for the pea enzyme are taken from Neuburger *et al.* (*40*).

carboxylate of Asp438. The amino of Lys160bd, a H2 residue, forms salt bridges with the carboxylates of Asp407′ and Glu437′. The carboxylate of Glu161bd, a H2 residue, forms a salt bridge with the guanidinium of Arg408′. The side chains of Lys433, Arg408′ and Phe340 that are involved in PSBD binding have conformations that differ from those of the other E3o subunit. The conformational alterations facilitate the formation of the intermolecular salt bridges and hydrophobic contacts. In addition to these salt bridges, there are two hydrogen bonds: the first, which is bridged by a water molecule, is between the carboxylate of Glu161bd and the hydroxyl of Thr406′. The second is between the main-chain NH of Ala134bd and the carboxylate of Asp438′, and is the only hydrophilic interaction that is conserved among all three E3•PSBDs.

Comparison of the E3•PSBD Structures—Superimposition of the three structures by least-squares fitting of only the Cα atoms of E3b and E3o shows a significant spatial deviation of PSBDo R2 in comparison with the positions of the other two PSBD R2s (Fig. 8); whereas pairwise least-squares fitting of the PSBD Cα atoms gives comparable rms deviations: 1.34 Å (PSBDp vs. PSBDb); 1.36 Å (PSBDb vs. PSBDo) and 1.48 Å (PSBDo vs. PSBDp). As described above, PSBDp and PSBDb bind in a similar manner to E3b, which is quite different from that found for PSBDo bound to E3o.

Certain interactions between the residues of E3b and PSBDp, and E3b and PSBDb are also found for *Gst* E3•*Gst* PSBDp (*28*): (i) All intermolecular salt bridges involve PSBD R1 residues. The salt bridges made by the guanidiniums of the R1 residues Arg136bd and Arg140bd are of central importance: the guanidinium of Arg136bd interacts with the E3 Asp344 and Glu431 carboxylates in all three complexes. The *Gst* Arg140bd guanidinium also participates in this salt-bridge network by interacting with the carboxylate of Asp344. [This series of interactions has been referred to as the 'electrostatic zipper' (*28*).] However, the guanidinium of Arg140bd in the *Tth* E3b•PSBDs forms a different salt bridge, one with Asp340. (ii) The R1 contribution to binding is greater than that of R2 for all three complexes. The R1 to R2 ratios of interface ASAs for PSBDp, PSBDb and *Gst* PSBDp are 6.8, 3.4 and 7.5, respectively. Additionally, none of the R2 residues form salt bridges with E3, which contrasts with what is found for the R1 residues.

The manner in which E3o and PSBDo bind is unlike those of the aforementioned complexes. This complex does not have the characteristic salt-bridge network in which Arg136bd plays a central role. Instead, the carboxylate of Glu136bd forms a weak electrostatic interaction with the amino of Lys433. For the PSBDo regions, the contribution of the R2 surface to binding is slightly greater than that of R1; the R1 to R2 interface ASA ratio is 0.9. Furthermore, the number of salt bridges between R2 and E3o is greater than that for R1 and E3o (Fig. 7 and Table S1). These differences are reflected in the features of the molecular surface buried in the E3•PSBDs. The charge distribution clearly differs for E3o•PSBDo and E3b•PSBDp/b (Fig. 6); although for all E3•PSBDs, the interface PSBD and E3 surfaces are predominantly positively and negatively charged, respectively. In addition, the molecular surfaces buried in each complex also differ in size and shape for E3o•PSBDo and E3b•PSBDp/b. These data strongly suggest that, for each E3•PSBD pair, the electrostatic and geometrical complementarities are responsible for the binding specificity.

Recently, the crystal structure of human E3•E3BD has been reported independently by two groups (*30*, *31*). Interestingly, this complex shares physical properties of both E3b•PSBDp/b and E3o•PSBD: (i) Human E3•E3BD has the characteristic salt-bridge between the R1 Arg136bd and the E3 Glu437, which corresponds to Glu431 of E3b. (ii) The R2 Lys160bd side chain forms salt bridges with Asp413′ and Glu443′, which correspond to Asp407′ and Glu437′ of E3o, respectively. Furthermore, the contribution of the R2 residues to binding is comparable with that of the R1 residues. The E3BD R1 to R2 interface ASA ratio is 1.4. However, there are no other hydrophilic interactions corresponding to those observed for any of the other four E3•PSBD complexes, excepting that between the main-chain NH of Ala134bd and the carboxylate of Asp444′, which corresponds to the Asp438 of E3b, E3o and *Gst* E3. This hydrogen bond is completely conserved among the E3•PSBDs and E3•E3BD.

CONCLUSIONS

In the present study, we found that each of the three E2 components of *Tth* 2-oxo acid dehydrogenases binds a specific E3 and that there are only three possible complexes (E3b•E2p, E3b•E2b and E3o•E2o). In contrast, when E3b and E3o act as the *Tth* GCS L-protein, neither of them exhibit specific interactions with the *Tth* H-protein and bind to it with similar affinities. Furthermore, we have analysed the crystal structures of the three E3•PSBD complexes, E3b•PSBDp, E3b•PSBDb and E3o•PSBDo, to elucidate the structural bases for the three specific complexes. In all E3•PSBDs, one PSBD binds to an E3 dimer through salt bridges, hydrogen bonds and hydrophobic interactions. The ways in which PSBDp and PSBDb bind E3b are quite similar, but unlike how PSBDo binds E3o. In all complexes, the buried molecular surfaces are predominantly positively (for PSBD) and negatively charged (for E3); however there are size, shape and charge distribution differences for E3o•PSBDo and E3b•PSBDp/b. Analysis of our data strongly suggests that the electrostatic and geometrical complementarities between the partner E3 and PSBD pairs are responsible for the binding specificities of the E3•PSBDs.

Supplementary material is available at *JB* online.

We thank Dr T. Hikima, Mr T. Matsu and Mr H. Nakajima (RIKEN SPring-8 Center) for their help with data collection at SPring-8. This work was supported by the RIKEN Structural Genomics/Proteomics Initiative (RSGI) of the National Project on Protein Structural and Functional Analyses, the Ministry of Education, Culture, Sports, Science, and Technology of Japan.

REFERENCES

1. Perham, R.N. (2000) Swinging arms and swinging domains in multifunctional enzymes: catalytic machines for multistep reactions. *Annu. Rev. Biochem.* **69**, 961–1004
2. Douce, R., Bourguignon, J., Neuburger, M., and Rebeille, F. (2001) The glycine decarboxylase system: a fascinating complex. *Trends Plant Sci.* **6**, 167–176
3. Bourguignon, J., Merand, V., Rawsthorne, S., Forest, E., and Douce, R. (1996) Glycine decarboxylase and pyruvate dehydrogenase complexes share the same dihydrolipoamide dehydrogenase in pea leaf mitochondria: evidence from mass spectrometry and primary-structure analysis. *Biochem. J.* **313**, 229–234
4. Ævarsson, A., Seger, K., Turley, S., Sokatch, J.R., and Hol, W.G. (1999) Crystal structure of 2-oxoisovalerate and dehydrogenase and the architecture of 2-oxo acid dehydrogenase multienzyme complexes. *Nat. Struct. Biol.* **6**, 785–792
5. Ævarsson, A., Chuang, J.L., Wynn, R.M., Turley, S., Chuang, D.T., and Hol, W.G. (2000) Crystal structure of human branched-chain alpha-ketoacid dehydrogenase and the molecular basis of multienzyme complex deficiency in maple syrup urine disease. *Structure Fold. Des.* **8**, 277–291
6. Nakai, T., Nakagawa, N., Maoka, N., Masui, R., Kuramitsu, S., and Kamiya, N. (2004) Ligand-induced conformational changes and a reaction intermediate in branched-chain 2-oxo acid dehydrogenase (E1) from *Thermus thermophilus* HB8, as revealed by X-ray crystallography. *J. Mol. Biol.* **337**, 1011–1033
7. Arjunan, P., Nemeria, N., Brunskill, A., Chandrasekhar, K., Sax, M., Yan, Y., Jordan, F., Guest, J.R., and Furey, W. (2002) Structure of the pyruvate dehydrogenase multienzyme complex E1 component from *Escherichia coli* at 1.85 Å resolution. *Biochemistry* **41**, 5213–5221
8. Ciszak, E.M., Korotchkina, L.G., Dominiak, P.M., Sidhu, S., and Patel, M.S. (2003) Structural basis for flip-flop action of thiamin pyrophosphate-dependent enzymes revealed by human pyruvate dehydrogenase. *J. Biol. Chem.* **278**, 21240–21246
9. Frank, R.A., Price, A.J., Northrop, F.D., Perham, R.N., and Luisi, B.F. (2007) Crystal structure of *Escherichia coli* 2-oxoglutarate dehydrogenase. *J. Mol. Biol.* **368**, 639–651
10. Mattevi, A., Schierbeek, A.J., and Hol, W.G. (1991) Refined crystal structure of lipoamide dehydrogenase from *Azotobacter vinelandii* at 2.2 Å resolution. A comparison with the structure of glutathione reductase. *J. Mol. Biol.* **220**, 975–994
11. Mattevi, A., Obmolova, G., Sokatch, J.R., Betzel, C., and Hol, W.G. (1992) The refined crystal structure of *Pseudomonas putida* lipoamide dehydrogenase complexed with NAD^+ at 2.45 Å resolution. *Proteins* **13**, 336–351
12. Mattevi, A., Obmolova, G., Kalk, K.H., van Berkel, W.J., and Hol, W.G. (1993) Three-dimensional structure of lipoamide dehydrogenase from *Pseudomonas fluorescens* at 2.8 Å resolution. Analysis of redox and thermostability properties. *J. Mol. Biol.* **230**, 1200–1215
13. Toyoda, T., Kobayashi, R., Sekiguchi, T., Koike, K., Koike, M., and Takenaka, A. (1998) Crystallization and preliminary X-ray analysis of pig E3, lipoamide dehydrogenase. *Acta Crystallogr. D Biol. Crystallogr.* **54**, 982–985
14. Toyoda, T., Suzuki, K., Sekiguchi, T., Reed, L.J., and Takenaka, A. (1998) Crystal structure of eucaryotic E3, lipoamide dehydrogenase from yeast. *J. Biochem.* **123**, 668–674
15. Faure, M., Bourguignon, J., Neuburger, M., MacHerel, D., Sieker, L., Ober, R., Kahn, R., Cohen-Addad, C., and Douce, R. (2000) Interaction between the lipoamide-containing H-protein and the lipoamide dehydrogenase (L-protein) of the glycine decarboxylase multienzyme system 2. Crystal structures of H- and L-proteins. *Eur. J. Biochem.* **267**, 2890–2898
16. Brautigam, C.A., Chuang, J.L., Tomchick, D.R., Machius, M., and Chuang, D.T. (2005) Crystal structure of human dihydrolipoamide dehydrogenase: NAD^+/NADH

binding and the structural basis of disease-causing mutations. *J. Mol. Biol.* **350**, 543–552
17. Rajashankar, K.R., Bryk, R., Kniewel, R., Buglino, J.A., Nathan, C.F., and Lima, C.D. (2005) Crystal structure and functional analysis of lipoamide dehydrogenase from *Mycobacterium tuberculosis*. *J. Biol. Chem.* **280**, 33977–33983
18. Dardel, F., Davis, A.L., Laue, E.D., and Perham, R.N. (1993) Three-dimensional structure of the lipoyl domain from *Bacillus stearothermophilus* pyruvate dehydrogenase multienzyme complex. *J. Mol. Biol.* **229**, 1037–1048
19. Berg, A., Vervoort, J., and de Kok, A. (1997) Three-dimensional structure in solution of the N-terminal lipoyl domain of the pyruvate dehydrogenase complex from *Azotobacter vinelandii*. *Eur. J. Biochem.* **244**, 352–360
20. Howard, M.J., Fuller, C., Broadhurst, R.W., Perham, R.N., Tang, J.G., Quinn, J., Diamond, A.G., and Yeaman, S.J. (1998) Three-dimensional structure of the major autoantigen in primary biliary cirrhosis. *Gastroenterology* **115**, 139–146
21. Jones, D.D., Horne, H.J., Reche, P.A., and Perham, R.N. (2000) Structural determinants of post-translational modification and catalytic specificity for the lipoyl domains of the pyruvate dehydrogenase multienzyme complex of *Escherichia coli*. *J. Mol. Biol.* **295**, 289–306
22. Ricaud, P.M., Howard, M.J., Roberts, E.L., Broadhurst, R.W., and Perham, R.N. (1996) Three-dimensional structure of the lipoyl domain from the dihydrolipoyl succinyltransferase component of the 2-oxoglutarate dehydrogenase multienzyme complex of *Escherichia coli*. *J. Mol. Biol.* **264**, 179–190
23. Robien, M.A., Clore, G.M., Omichinski, J.G., Perham, R.N., Appella, E., Sakaguchi, K., and Gronenborn, A.M. (1992) Three-dimensional solution structure of the E3-binding domain of the dihydrolipoamide succinyltransferase core from the 2-oxoglutarate dehydrogenase multienzyme complex of *Escherichia coli*. *Biochemistry* **31**, 3463–3471
24. Kalia, Y.N., Brocklehurst, S.M., Hipps, D.S., Appella, E., Sakaguchi, K., and Perham, R.N. (1993) The high-resolution structure of the peripheral subunit-binding domain of dihydrolipoamide acetyltransferase from the pyruvate dehydrogenase multienzyme complex of *Bacillus stearothermophilus*. *J. Mol. Biol.* **230**, 323–341
25. Mattevi, A., Obmolova, G., Schulze, E., Kalk, K.H., Westphal, A.H., de Kok, A., and Hol, W.G. (1992) Atomic structure of the cubic core of the pyruvate dehydrogenase multienzyme complex. *Science* **255**, 1544–1550
26. Knapp, J.E., Mitchell, D.T., Yazdi, M.A., Ernst, S.R., Reed, L.J., and Hackert, M.L. (1998) Crystal structure of the truncated cubic core component of the *Escherichia coli* 2-oxoglutarate dehydrogenase multienzyme complex. *J. Mol. Biol.* **280**, 655–668
27. Izard, T., Ævarsson, A., Allen, M.D., Westphal, A.H., Perham, R.N., de Kok, A., and Hol, W.G. (1999) Principles of quasi-equivalence and Euclidean geometry govern the assembly of cubic and dodecahedral cores of pyruvate dehydrogenase complexes. *Proc. Natl. Acad. Sci. USA* **96**, 1240–1245
28. Mande, S.S., Sarfaty, S., Allen, M.D., Perham, R.N., and Hol, W.G. (1996) Protein-protein interactions in the pyruvate dehydrogenase multienzyme complex: dihydrolipoamide dehydrogenase complexed with the binding domain of dihydrolipoamide acetyltransferase. *Structure* **4**, 277–286
29. Frank, R.A., Pratap, J.V., Pei, X.Y., Perham, R.N., and Luisi, B.F. (2005) The molecular origins of specificity in the assembly of a multienzyme complex. *Structure* **13**, 1119–1130
30. Ciszak, E.M., Makal, A., Hong, Y.S., Vettaikkorumakankauv, A.K., Korotchkina, L.G., and Patel, M.S. (2006) How dihydrolipoamide dehydrogenase-binding protein binds dihydrolipoamide dehydrogenase in the human pyruvate dehydrogenase complex. *J. Biol. Chem.* **281**, 648–655
31. Brautigam, C.A., Wynn, R.M., Chuang, J.L., Machius, M., Tomchick, D.R., and Chuang, D.T. (2006) Structural insight into interactions between dihydrolipoamide dehydrogenase (E3) and E3 binding protein of human pyruvate dehydrogenase complex. *Structure* **14**, 611–621
32. Oliver, D.J., Neuburger, M., Bourguignon, J., and Douce, R. (1990) Interaction between the component enzymes of the glycine decarboxylase multienzyme complex. *Plant Physiol.* **94**, 833–839
33. Nakai, T., Nakagawa, N., Maoka, N., Masui, R., Kuramitsu, S., and Kamiya, N. (2005) Structure of P-protein of the glycine cleavage system: implications for nonketotic hyperglycinemia. *EMBO J.* **24**, 1523–1536
34. Cohen-Addad, C., Pares, S., Sieker, L., Neuburger, M., and Douce, R. (1995) The lipoamide arm in the glycine decarboxylase complex is not freely swinging. *Nat. Struct. Biol.* **2**, 63–68
35. Nakai, T., Ishijima, J., Masui, R., Kuramitsu, S., and Kamiya, N. (2003) Structure of *Thermus thermophilus* HB8 H-protein of the glycine-cleavage system, resolved by a six-dimensional molecular-replacement method. *Acta Crystallogr. D Biol. Crystallogr.* **59**, 1610–1618
36. Lee, H.H., Kim, D.J., Ahn, H.J., Ha, J.Y., and Suh, S.W. (2004) Crystal structure of T-protein of the glycine cleavage system: Cofactor binding, insights into H-protein recognition, and molecular basis for understanding nonketotic hyperglycinemia. *J. Biol. Chem.* **279**, 50514–50523
37. Lokanath, N.K., Kuroishi, C., Okazaki, N., and Kunishima, N. (2005) Crystal structure of a component of glycine cleavage system: T-protein from *Pyrococcus horikoshii* OT3 at 1.5 Å resolution. *Proteins* **58**, 769–773
38. Okamura-Ikeda, K., Hosaka, H., Yoshimura, M., Yamashita, E., Toma, S., Nakagawa, A., Fujiwara, K., Motokawa, Y., and Taniguchi, H. (2005) Crystal structure of human T-protein of glycine cleavage system at 2.0 Å resolution and its implication for understanding non-ketotic hyperglycinemia. *J. Mol. Biol.* **351**, 1146–1159
39. Yokoyama, S., Hirota, H., Kigawa, T., Yabuki, T., Shirouzu, M., Terada, T., Ito, Y., Matsuo, Y., Kuroda, Y., Nishimura, Y., Kyogoku, Y., Miki, K., Masui, R., and Kuramitsu, S. (2000) Structural genomics projects in Japan. *Nat. Struct. Biol.* **7**, 943–945
40. Neuburger, M., Polidori, A.M., Pietre, E., Faure, M., Jourdain, A., Bourguignon, J., Pucci, B., and Douce, R. (2000) Interaction between the lipoamide-containing H-protein and the lipoamide dehydrogenase (L-protein) of the glycine decarboxylase multienzyme system. 1. Biochemical studies. *Eur. J. Biochem.* **267**, 2882–2889
41. Yamamoto, M., Kumasaka, T., Fujisawa, T., and Ueki, T. (1998) Trichromatic concept at SPring-8 RIKEN beamline I. *J. Synchrot. Radiat.* **5**, 222–225
42. Adachi, S., Oguchi, T., Tanida, H., Park, S.Y., Shimizu, H., Miyatake, H., Kamiya, N., Shiro, Y., Inoue, Y., Ueki, T., and Iizuka, T. (2001) The RIKEN structural biology beamline II (BL44B2) at the SPring-8. *Nucl. Instrum. Methods Phys. Res. Sect. A-Accel. Spectrom.* **467**, 711–714
43. Otwinowski, Z. and Minor, W. (1997) Processing of X-ray diffraction data collected in oscillation mode. *Methods Enzymol.* **276**, 307–326
44. Navaza, J. (1994) AMoRe: an automated package for molecular replacement. *Acta Crystallogr. Sect. A* **50**, 157–163
45. Brunger, A.T., Adams, P.D., Clore, G.M., DeLano, W.L., Gros, P., Grosse-Kunstleve, R.W., Jiang, J.S., Kuszewski, J., Nilges, M., Pannu, N.S., Read, R.J., Rice, L.M., Simonson, T., and Warren, G.L. (1998) Crystallography &

NMR system: A new software suite for macromolecular structure determination. *Acta Crystallogr. D Biol. Crystallogr.* **54**, 905–921
46. McRee, D.E. (1992) A visual protein crystallographic software system for X11/XView. *J. Mol. Graphics* **10**, 44–46
47. Kraulis, P.J. (1991) MOLSCRIPT: a program to produce both detailed and schematic plots of protein structures. *J. Appl. Crystallogr.* **24**, 946–950
48. Nicholls, A., Sharp, K.A., and Honig, B. (1991) Protein folding and association: insights from the interfacial and thermodynamic properties of hydrocarbons. *Proteins* **11**, 281–296
49. Merritt, E.A. and Bacon, D.J. (1997) Raster3D photorealistic molecular graphics. *Methods Enzymol.* **277**, 505–524
50. Sokatch, J.R. and Burns, G. (1984) Oxidation of glycine by *Pseudomonas putida* requires a specific lipoamide dehydrogenase. *Arch. Biochem. Biophys.* **228**, 660–666
51. Fries, M., Stott, K.M., Reynolds, S., and Perham, R.N. (2007) Distinct modes of recognition of the lipoyl domain as substrate by the E1 and E3 components of the pyruvate dehydrogenase multienzyme complex. *J. Mol. Biol.* **366**, 132–139
52. Perham, R.N. (1991) Domains, motifs, and linkers in 2-oxo acid dehydrogenase multienzyme complexes: a paradigm in the design of a multifunctional protein. *Biochemistry* **30**, 8501–8512
53. Spector, S., Kuhlman, B., Fairman, R., Wong, E., Boice, J.A., and Raleigh, D.P. (1998) Cooperative folding of a protein mini domain: the peripheral subunit-binding domain of the pyruvate dehydrogenase multienzyme complex. *J. Mol. Biol.* **276**, 479–489